Chinese Chemical Letters 34 (2023) 107634

Contents lists available at ScienceDirect

Chinese Chemical Letters

journal homepage: www.elsevier.com/locate/cclet

Acceptor modulation for improving thermally activated delayed fluorescence emitter in through-space charge transfer on spiroskeletons

Jingfeng Liu[a,1], Ziqi Feng[a,1], Chenchen Peng[a], Youjun Yu[a], Shengyi Yang[a], Zuoquan Jiang[a,*], Liangsheng Liao[a,b,*]

[a] Institute of Functional Nano & Soft Materials (FUNSOM), Jiangsu Key Laboratory for Carbon-Based Functional Materials & Devices, Soochow University, Suzhou 215123, China
[b] Macao Institute of Materials Science and Engineering, Macau University of Science and Technology, Taipa 999078, Macau SAR, China

ARTICLE INFO

Article history:
Received 26 April 2022
Revised 3 June 2022
Accepted 21 June 2022
Available online 26 June 2022

Keywords:
Thermally activated delayed fluorescence
Organic light-emitting diodes
Through-space charge transfer
Acceptor modulation
Spiro skeleton

ABSTRACT

Through-space charge transfer (TSCT) is regarded as an effective way to develop thermally activated delayed fluorescence (TADF) emitters. Based on this strategy, many molecular frameworks have been proposed, among which spirobased scaffolds have been extensively studied due to their unique advantages. In this work, we developed three emitters SPS, SPO, and SPON, which were constructed with the same donor and various acceptors to explore the influence of acceptor modulation at the C9 position of fluorene for spirostructure TSCT emitters. The results show that the acceptor with too weak electron-withdrawing ability will cause the emitter to not have TADF properties, while the acceptor with too much steric hindrance will weaken the face-to-face π-π stacking interaction between donor/acceptor (D/A). Since SPO balances the electron-withdrawing strength and steric hindrance of the acceptor, it achieves the highest external quantum efficiency (EQE) of 17.75%. This work shows that appropriate acceptor selection is essential for the TADF properties and high efficiency of the spirobased scaffold TSCT emitter

In the past decade, organic light-emitting diodes (OLEDs) have developed rapidly due to the proposal of thermally activated delayed fluorescence (TADF) [1–7]. It is different from fluorescence emitters that only have 25% exciton utilization and phosphorescent emitters that require the use of noble metals to achieve 100% exciton utilization, TADF emitters of the pure organic component can utilize whole excitons in the singlet/triplet states through reverse intersystem crossing (RISC) process under the action of environmental heat to achieve 100% exciton utilization [8,9]. The concept of TADF was first proposed by Adachi *et al.*, at the same time, they also constructed the TADF molecule design concept of the donor (D)-π-acceptor (A) structure. This design is advantageous in flexibly adjusting the D or/and A moieties, geometry, and steric hindrance of the molecule to produce a distorted dihedral angle between D/A moieties, which makes a smaller the lowest excited singlet (S_1) and triplet (T_1) energy gap (ΔE_{ST}) for fast RISC process [10].

Besides the classic D-π-A conformation, recently, researchers have discovered that the face-to-face alignment based on D/A non-conjugation interaction is also an effective strategy to realize TADF. By connecting donor and acceptor at different positions in the same direction of the rigid linker, the D/A can be sufficiently separated to obtain a very small ΔE_{ST} value, meanwhile, the D/A can be kept close in space to form homoconjugation. This concept is defined as through-space charge transfer (TSCT). Many molecular frameworks suited for TSCT have been proposed [11–16] and the spiroskeleton is progressing more quickly as it can serve as a rigid backbone to hold a donor at the spiroposition and restrict acceptor at the neighboring position [17–20]. As shown in Fig. 1, Our group has investigated different acceptor at C1 site of fluorene framework in separated reports and found that the luminescence mechanism is deeply associated with the acceptors [21–23].

Herein, we collectively explore the influence of acceptor modulation at the C9 site of fluorene scaffold for TSCT emitters (Fig. 1). Three different electron-withdrawing groups: sulfonyl diphenyl, benzophenone, and phenyl(pyridin-2-yl) ketone were selected as acceptors to construct the spiroskeleton through cyclization. They all bond the same donor moiety, benzo[5,6][1,4]oxazine[2,3,4-

* Corresponding authors.
E-mail addresses: zqjiang@suda.edu.cn (Z. Jiang), lsliao@suda.edu.cn (L. Liao).
[1] These authors contributed equally to this work.

https://doi.org/10.1016/j.cclet.2022.06.057
1001-8417/

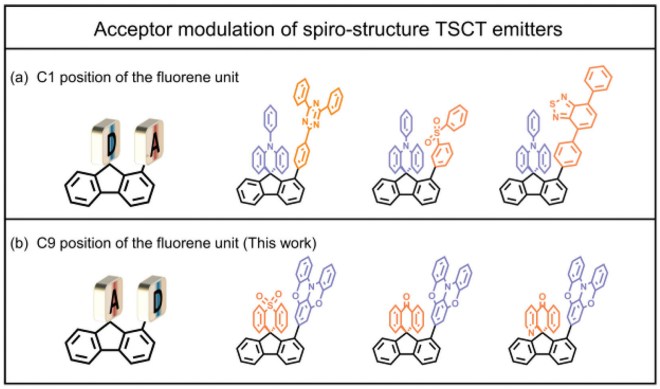

Fig. 1. Acceptor modulated molecules: (a) C1 position of the fluorene unit and (b) C9 position in this investigation.

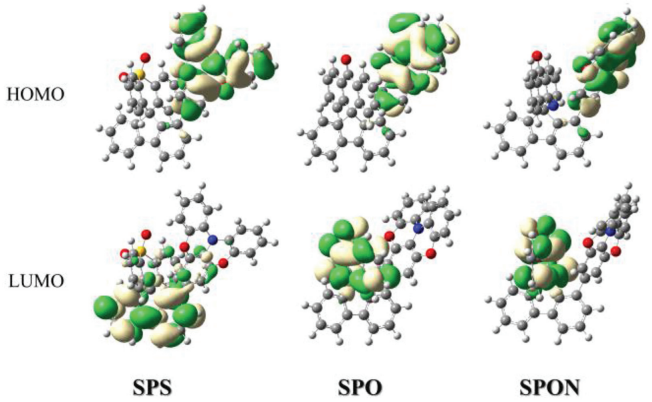

Fig. 2. The molecular structures and energy level distributions of SPS, SPO and SPON.

kl]phenoxazine (TAPO) at the C1 site of the fluorene unit to synthesize three TSCT emitters, named SPS, SPO, and SPON, respectively. As a result, the maximum external quantum efficiencys (EQE)s of SPS-, SPO- and SPON-based devices are 8.5%, 17.8% and 14.4%, respectively. We found that due to the relatively weak electron-drawing ability of the sulfonyl diphenyl unit, the highest occupied molecular orbital (HOMO) and the lowest occupied molecular orbital (LUMO) of SPS cannot be separated, so SPS does not have TADF properties. However, with the enhancement of the electron-withdrawing ability of the acceptor, the HOMO-LUMOs of SPO and SPON are completely separated and exhibited significant TADF properties. The acceptor of SPON has the strongest electron-withdrawing ability, but the larger steric hindrance increases the D/A distance and weakens the face-to-face π-π stacking interaction. SPO achieves a good balance of acceptor strength and steric hindrance, thus achieving the highest efficiency. This work shows that suitable acceptor selection at the C9 position of fluorene unit is important for adjusting the TADF properties and electroluminescence (EL) efficiency of spirobased scaffold TSCT materials, which also provides new ideas for the design of TADF emitters.

The synthetic routes of SPS, SPO and SPON are shown in Scheme S1 (Supporting information). From 9-fluorenone-1-boronic acid, intermediate **1** was prepared through Suzuki-Miyaura palladium-catalyzed cross-coupling reaction. Then, we used nucleophilic addition reaction and Friedel–Crafts cyclization reaction to form intermediates **2**, **3** and **4** with a spiroskeleton. Finally, the final product SPS, SPO and SPON were synthesized through an oxidation reaction. The chemical structures of all molecules have been characterized by ^{1}H NMR, ^{13}C NMR (Figs. S1-S14 in Supporting information) and mass spectrometry. The chemical structures of the final product SPS, SPO and SPON were further characterized by elemental analysis and single-crystal X-ray diffraction analysis (XRD).

The single crystals of SPS, SPO, and SPON were obtained by solvent diffusion in a mixed solvent of methanol and tetrahydrofuran (Tables S1-S3 in Supporting information). As shown in Fig. S15 (Supporting information), the donor unit and acceptor unit of the three molecules all exhibit a close face-to-face stacking, and the D/A distances are in the range of 2.98–3.17 Å. For SPS, the D/A distance (d) is 2.982 Å, and the dihedral angle (φ) between the respective planes of D and A is 16.11°, indicating a close face-to-face D/A alignment. However, the LUMO of SPS is delocalized on the fluorene unit, and the fluorene unit as the real acceptor directly interacts with the donor intramolecularly, rather than interacting in space. For SPO, due to the larger steric hindrance of the benzophenone unit, the d and φ of SPO are larger than SPS, which are 3.158 Å and 36.25°, respectively. For SPON, the acceptor has the largest steric hindrance among the three molecules, so d is the largest at 3.170 Å. However, the strong electron-withdrawing ability of the acceptor reduces the φ to 17.53° The single-crystal structures show that the three emitters all exhibit strong or sizable face-to-face D/A π-π stacking interactions, the dihedral angle between the respective planes of the donor and acceptor indicates that the three molecules all exhibit a face-to-face D/A arrangement, both are very conducive to the spatial interaction between the donor and acceptor.

To gain a detailed insight into the electronic structures of the three emitters, density functional theory (DFT) and time-dependent density functional theory (TD-DFT) calculations have been performed to simulate their frontier orbital distributions. As shown in Fig. 2, the HOMOs of SPS, SPO, and SPON are all distributed on the same donor unit, while their LUMOs distribution is different due to the disparate acceptors. Be owing to the weak electron-withdrawing ability of the sulfonyl diphenyl unit, the LUMO of SPS is mainly distributed on the rigid linker fluorene. As a result, the HOMO-LUMO of SPS cannot be completely separated, and the ΔE_{ST} of SPS is large, which is 0.40 eV. For SPO and SPON, due to the strong electron-withdrawing ability of the acceptors, LUMOs can completely delocalize on their acceptors, and the fluorene unit acts as a rigid linker as we imagined. Therefore, the HOMO-LUMOs of SPO and SPON are completely separated, and their ΔE_{ST}s are very small, both of which are 0.01 eV. At the same time, the LUMOs of SPS, SPO, and SPON gradually decreased due to the gradual increase in the electron-withdrawing ability of their acceptors, which are −1.13, −1.69 and −1.91 eV, respectively, the detailed data is shown in Table S4 (Supporting information).

The photophysical properties of the three emitters were explored in oxygen-free toluene (10^{-5} mol/L) solution and summarized in Table S5 (Supporting information). As shown in Fig. 3a, the absorption spectra of the emitters have two main absorption bands, the strong absorption band near 310 nm is attributed to the local π-π^* and n-π^* transitions of the conjugation skeleton, and the weak absorption band near 360 nm is originated from the intramolecular charge transfer (ICT) between their donor and acceptor units. The emission peaks of SPS, SPO and SPON are 455, 525 and 450/570 nm, respectively. As shown in Fig. 3b, the emission peaks at short wavelengths of SPON, the emission peak of TPAO-linked fluorene fragment (the fragment is named SD), and the emission peak of SPS, the wavelengths of these three emission peaks are the same. The photophysical properties of the three emitters were further explored in different polar solvents. As shown in Fig. S16 (Supporting information), SPO and SPON both exhibit double emission in different solvents, and the emission peaks are red-shifted with increasing solvent polarity. These results indicate that the short-wavelength emission peaks of SPO and SPON are caused by the charge transfer excited state between the

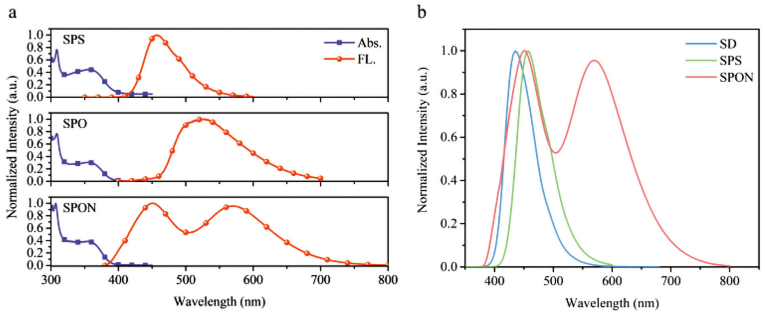

Fig. 3. (a) Absorption and PL spectra of SPS, SPO and SPON. (b) PL spectra of SD, SPS and SPON in toluene solution (10^{-5} mol/L).

donor TPAO unit and the fluorene (wavelength varies with solvent polarity), and the long-wavelength emission peak is due to the charge transfer excited state of the donor and acceptor (the wavelength is significantly red-shifted with increasing solvent polarity). Therefore, it is reasonable to think that the dual emission of SPO and SPON is due to the incomplete energy transfer of the molecule due to the highly twisted spirobackbone, resulting in the emergence of higher-level emission [24]. In the oxygen-free toluene solution, the photoluminescence quantum yields (PLQYs) of the three emitters are less than 10%, indicating that there is a considerable non-radiation decay loss in the fluid solution, which may be caused by the vibration or rotation of the unfixed TPAO unit. Based on the starting points of the fluorescence and phosphorescence spectra (Fig. S17 in Supporting information) of the three emitters in 77 K toluene solution, the ΔE_{ST}s of SPS, SPO, and SPON were calculated to be 0.49, 0.04 and 0.01 eV, respectively, the results have the same regularity as the theoretical calculation results.

The solid-state photoluminescence (PL) properties of SPS, SPO, and SPON have been explored in dopant films. We chose our own synthetic emitter OPPC as host and prepared three doped films by doping 12 wt% of the emitters in OPPC. As shown in Fig. S18 (Supporting information), the three films all exhibit a single emission, respectively. According to the photophysical properties in the solution, it can be inferred that the single emission of the SPO- and SPON-based film originates from the through space charge transfer state, indicating the solid film creates a more rigid environment for SPO and SPON and inhibits the charge transfer between the fluorene unit and the TPAO unit. The PLQYs of the three dopant films were measured to be 91.2% for SPS, 72.4% for SPO, and 89.4% for SPON, respectively. Compared with in solution, the PLQYs of the doped films exhibit significant improvement, indicating that the vibration or rotation of molecules is well restricted in solid-state [25]. To further confirm the TADF characteristics of the three emitters, we have explored their transient PL spectra in dopant films. As shown in Fig. S19 (Supporting information), SPO and SPON have obvious delayed components, while SPS has only prompted components, indicating the obvious TADF nature of SPO and SPO, and further confirming that SPS is a fluorescent emitter.

Good thermal stability is a necessary property of the luminescent material to prevent the emitter from decomposing or changing in the process of thermal evaporation. The thermal properties of three emitters were tested by thermo-gravimetric analysis (TGA) and differential scanning calorimeter (DSC) under an N_2 atmosphere. As shown in Fig. S20 (Supporting information), the thermal decomposition temperature (T_d, defined as the temperature at which weight loss is 5%) of SPS, SPO and SPON are 412, 328, and 383 °C, respectively, the glass transition temperature (T_g) are 154, 144 and 158 °C, respectively, and the detailed data are listed in Table S6 (Supporting information). The rigid structure of the spiral ring makes the three emitters have excellent thermal stability and morphological stability, which is very beneficial to the manufacture of thermal evaporation devices.

The electrochemical properties of the three emitters were tested by cyclic voltammetry using ultra-dry dichloromethane as solvent and ferrocene as an internal reference. The test results are shown in Fig. S21 (Supporting information), and the detailed data are listed in Table S6 (Supporting information). According to the empirical formulas $E_{HOMO} = -(E_{ox} + 4.8 - E_{fc})$ and $E_{LUMO} = -(E_{re} + 4.8 - E_{fc})$, E_{ox} and E_{re} are the oxidation potential and reduction potential of the three emitters, respectively, and E_{fc} is the oxidation–reduction potential of ferrocene. It was calculated that the HOMO energy levels of SPS, SPO and SPON are −5.01, −5.03 and −5.04 eV, respectively, and the LUMO energy levels are −2.33, −2.51 and −2.59 eV, respectively. Then according to the empirical formula $E_{LUMO} - E_{HOMO} = \Delta E_g$, the band gaps of SPS, SPO and SPON were calculated to be 2.68, 2.52 and 2.45 eV, respectively. Since the donor of the three emitters is the same moiety, their HOMO energy levels are similar. At the same time, the LUMO energy levels of SPS, SPO and SPON are gradually decreased due to the gradual enhancement of the electron-withdrawing ability of their acceptors.

To explore the electroluminescence (EL) performance of SPS, SPO and SPON, the OLEDs were fabricated with a normal sandwiched structure of indium tin oxide (ITO)/1,4,5,8,9,11-hexaazatriphenylene hexacarbonitrile (HAT-CN, 10 nm)/1,1-bis[4-[*N*,*N*-di(*p*-tolyl)amino]phenyl]-cyclohexane (TAPC, 40 nm)/tris(4-carbazolyl-9-ylphenyl)amine (TCTA, 10 nm)/EML (20 nm)/4,6-bis(3,5-di(yridine-4-yl)phenyl)−2-phenylpyrimidine (TmPyPB, 40 nm)/8-hydroxyquinolinolato lithium (Liq, 3 nm)/Al (60 nm). D1, D2, D3 represent SPS, SPO and SPON-based devices, respectively. HAT-CN, TAPC and TCTA were utilized as the hole-injecting layer (HIL), hole-transporting layer (HTL), and exciton blocking layer, respectively. TmPyPB and Liq were served as the electron-transporting layer (ETL) and electron-injecting layer (EIL), respectively. Emitters were doped into OCPC with 12 wt% were used as the emitting layer (EML). The molecular structure, configuration, and energy level alignment of OLEDs are shown in Fig. S22 (Supporting information). The EQE–Luminance curves, EL spectra, Current Efficiency, and Current density–Voltage–Radiance curves of SPS, SPO, and SPON are shown in Fig. 4 and summarized in Table S7 (Supporting information). The maximum EQEs (EQE_{max}s) of D1, D2, D3 are 8.5%, 17.8% and 14.4%, respectively, and the corresponding emission peaks are 520, 528 and 552 nm, respectively. At 1000 cd/m^2, the EQEs of the D1, D2 and D3 are 2.01%, 14.23% and 12.74%, respectively, and the corresponding efficiency roll-offs are 76%, 19% and 11%, respectively. D2 and D3 exhibit small efficiency roll-offs, while D1 has large efficiency roll-offs. For D1, due to the SPS guest having no TADF feature, so its efficiency is low. For D2 and D3, since the doped film of SPO has a higher PLQY and the D/A distance of SPO is smaller, the efficiency of D2 is the highest.

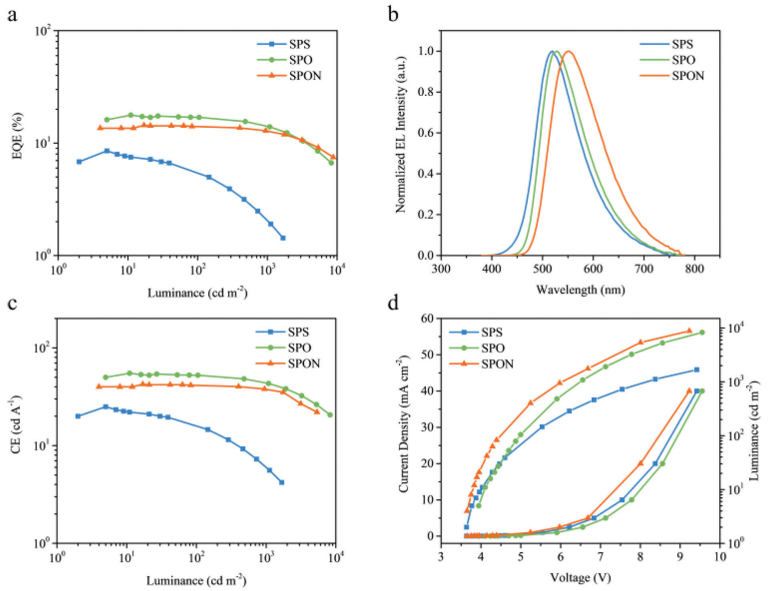

Fig. 4. (a) EQE–luminance curves, (b) EL spectra, (c) current efficiency and (d) current density–voltage–radiance curves of SPS, SPO and SPON.

In summary, we have developed three spirobased scaffold TSCT emitters with the same donor and different acceptors namely, SPS, SPO, and SPON. Combining theoretical calculations, single-crystal structure, photophysical properties, and electroluminescence properties, the influence of acceptor modulation at the C9 site of fluorene scaffold for spirobased scaffold TSCT emitters has been systematically studied. Eventually, OLEDs based on SPS, SPO and SPON exhibit EQEmaxs and emission peaks of 8.5% and 520 nm, 17.8% and 528 nm, 14.4% and 552 nm, respectively. The results show that the acceptor with weak electron-withdrawing ability will cause the LUMO can only delocalize on the rigid substrate, the acceptor and donor cannot perform TSCT interactions. The acceptor with strong electro-withdrawing ability will increase the D/A distance due to excessive steric hindrance and weaken the face-to-face $\pi-\pi$ stacking interactions. Therefore, due to moderate acceptor strength and steric hindrance of SPO, SPO-based OLED achieve the best efficiency. This work indicates that balancing the electron-withdrawing strength and steric hindrance of the acceptor is pivotal for adjusting the TADF properties and EL efficiency of spirobased scaffold TSCT emitters.

Declaration of competing interest

The authors declare no conflict of interest.

Acknowledgments

The authors acknowledge financial support from the National Natural Science Foundation of China (Nos. 51773141, 51873139, 61961160731, 62175171 and 22175124). This project is also funded by the Suzhou Science and Technology Plan Project (No. SYG202010). This work is also supported by Suzhou Key Laboratory of Functional Nano & Soft Materials, Collaborative Innovation Center of Suzhou Nano Science & Technology, the 111 Project, Joint International Research Laboratory of Carbon-Based Functional Materials and Devices.

Supplementary materials

Supplementary material associated with this article can be found, in the online version, at doi:10.1016/j.cclet.2022.06.057.

References

[1] Y.K. Chen, J. Jayakumar, C.M. Hsieh, et al., Adv. Mater. 33 (2021) e2008032.
[2] Y. Chen, D. Zhang, Y. Zhang, et al., Adv. Mater. 33 (2021) e2103293.
[3] S. Oda, B. Kawakami, Y. Yamasaki, et al., J. Am. Chem. Soc. 144 (2022) 106–112.
[4] H. Lim, S.J. Woo, Y.H. Ha, Y.H. Kim, J.J. Kim, Adv. Mater. 34 (2022) e2100161.
[5] R. Jiang, X. Wu, H. Liu, et al., Adv. Sci. 9 (2022) e2104435.
[6] Y.K. Qu, Q. Zheng, J. Fan, L.S. Liao, Z. Q. Jiang, Acc. Mater. Res. 2 (2021) 1261–1271.
[7] S.Y. Yang, Y.K. Qu, L.S. Liao, Z.Q. Jiang, S.T. Lee, Adv. Mater. (2021) 2104125.
[8] Y. Tao, K. Yuan, T. Chen, et al., Adv. Mater. 26 (2014) 7931–7958.
[9] Z. Yang, Z. Mao, Z. Xie, et al., Chem. Soc. Rev. 46 (2017) 915–1016.
[10] G. Méhes, H. Nomura, Q. Zhang, T. Nakagawa, C. Adachi, Angew. Chem. Int. Ed. 51 (2012) 11311–11315.
[11] S. Shao, J. Hu, X. Wang, L. Wang, X. Jing, F. Wang, J. Am. Chem. Soc. 139 (2017) 17739–17742.
[12] J. Li, Y.H. Li, Y. Zhao, et al., Org. Electron. 54 (2018) 140–147.
[13] C. Yin, D. Zhang, Y. Zhang, et al., CCS Chem. 2 (2020) 1268–1277.
[14] M. Auffray, U. Balijapalli, J.C. Ribierre, Y. Tsuchiya, C. Adachi, Chem. Lett. 49 (2020) 932–935.
[15] C. Wu, W. Liu, K. Li, et al., Angew. Chem. Int. Ed. 60 (2021) 3994–3998.
[16] T. Huang, Q. Wang, S. Xiao, et al., Angew. Chem. Int. Ed. 60 (2021) 23771–23776.
[17] Y. Song, M. Tian, R. Yu, L. He, ACS Appl. Mater. Interfaces 13 (2021) 60269–60278.
[18] X.Q. Wang, S.Y. Yang, Q.S. Tian, et al., Angew. Chem. Int. Ed. 60 (2021) 5213–5219.
[19] H. Liu, Z. Liu, G. Li, et al., Angew. Chem. Int. Ed. 60 (2021) 12376–12380.
[20] H.C. Li, X. Tang, S.Y. Yang, et al., Chin. Chem. Lett. 32 (2021) 1245–1248.
[21] X. Tang, L.S. Cui, H.C. Li, et al., Nat. Mater. 19 (2020) 1332–1338.
[22] S.Y. Yang, Q.S. Tian, Y.J. Yu, et al., J. Org. Chem. 85 (2020) 10628–10637.
[23] S.Y. Yang, Y.L. Zhang, F.C. Kong, et al., Chem. Eng. J. 418 (2021) 129366.
[24] X. Gong, C.H. Lu, W.K. Lee, et al., Chem. Eng. J. 405 (2021) 126663.
[25] J.A. Lin, S.W. Li, Z.Y. Liu, et al., Chem. Mater. 31 (2019) 5981–5992.